View Article Online / Journal Homepage / Table of Contents for this issue
Dynamic Article Links

PCCP

Cite this: *Phys. Chem. Chem. Phys.*, 2012, **14**, 1175–1184

www.rsc.org/pccp

PAPER

Calculation of two-photon absorption strengths with the approximate coupled cluster singles and doubles model CC2 using the resolution-of-identity approximation

Daniel H. Friese,*[a] Christof Hättig[a] and Kenneth Ruud[b]

Received 26th September 2011, Accepted 4th November 2011
DOI: 10.1039/c1cp23045j

An implementation of two-photon absorption matrix elements using the approximate second-order coupled-cluster singles and doubles model CC2 is presented. In this implementation we use the resolution-of-the-identity approximation for the two-electron repulsion integrals to reduce the computational cost. To avoid storage of large arrays we introduce in addition a numerical Laplace transformation of orbital energy denominators for the response of the doubles amplitudes. The error due to the numerical Laplace transformation is found to be negligible. Using this new implementation, we performed a series of benchmark calculations on substituted benzene and azobenzene derivatives to get reference values for TD-DFT results. We show that results obtained with the Coulomb-attenuated B3LYP functional are in reasonable agreement with the coupled-cluster results, whereas other density functionals which do not have a long-range correction give considerably less accurate results. Applications to the AF240 dye molecule and a weakly bound molecular tweezer complex demonstrate that this new RI-CC2 implementation allows for the first time to compute two-photon absorption cross sections with a correlated wave function method for molecules with more than 70 atoms and to apply this method for benchmarking TD-DFT calculations on molecules which are of particular relevance for experimental studies of two-photon absorption.

Published on 30 November 2011. Downloaded by Ruhr Universitat Bochum on 12/22/2018 1:15:42 PM.

1 Introduction

After having been predicted by Maria Göppert-Mayer[1] in 1931 and its first experimental realization in 1961,[2] two-photon absorption has been of interest both for science and for various technological applications.[3] Since high absorption cross sections in general are observed mainly on larger chromophores, the treatment of two-photon absorption is a challenge for quantum chemistry. When it comes to excited states of larger molecules, time-dependent density functional theory (TD-DFT) is widely used.[4] However, TD-DFT is well known both from calculated results[5,6] and from theory[7] to have challenges, especially in the treatment of charge-transfer excitations. The development of *ab initio* methodology that allows for a reliable evaluation of excited-state properties therefore continues to be important.

In this work we present an implementation of two-photon absorption matrix elements using the well-established second-order approximate coupled-cluster singles and doubles model CC2[8] in combination with the resolution-of-identity approximation for the treatment of two-electron integrals.[9] This allows us for the first time to perform correlated wave function-based calculations of two-photon absorption cross sections on molecules with more than 70 atoms using reasonable basis sets.

Our implementation is tested on a set of molecules which have previously been studied using the Coulomb-attenuated B3LYP functional (CAM-B3LYP).[10] In these calculations, CC2 is used as a benchmark for TD-DFT. As a non-linear optical property, two-photon absorption cross sections are much more sensitive to the choice of the electronic structure method than (one-photon) oscillator strengths and other linear optical properties. Different methods and different density functionals often give results which are not even in qualitative agreement.[11]

It is thus of particular interest to compare the results obtained with typical density functionals with those of a correlated wave function method, CC2, which often gives results close to those of higher-order methods, for some molecules with chromophores relevant also for experimental TPA studies.[11]

The remainder of this paper is organized as follows: In Section 2 we summarize the working equations for the calculation of two-photon absorption strengths within the RI-CC2 approach.

[a] *Lehrstuhl für Theoretische Chemie, Ruhr-Universität Bochum, D-44801 Bochum, Germany. E-mail: daniel.friese@rub.de, christof.haettig@rub.de*
[b] *Centre for Theoretical and Computational Chemistry, Department of Chemistry, University of Tromsø, N–9037 Tromsø, Norway. E-mail: kenneth.ruud@uit.no*

View Article Online

Published on 30 November 2011. Downloaded by Ruhr Universitat Bochum on 12/22/2018 1:15:42 PM.

In Section 3 we describe the details of our calculations, before we in Section 4 present the results. Finally, in Section 5 we give some concluding remarks.

2 Theory

The two-photon absorption matrix elements between the ground state $\langle 0|$ and an excited state $\langle J|$ are defined as:[12,13]

$$M^{XY}_{0\leftarrow J} = \hat{P}^{XY} \sum_K \frac{\langle 0|X|K\rangle\langle K|Y|J\rangle}{(\omega_X - \omega_K)}, \quad (1)$$

$$M^{XY}_{J\leftarrow 0} = \hat{P}^{XY} \sum_K \frac{\langle J|X|K\rangle\langle K|Y|0\rangle}{(\omega_X - \omega_K)}, \quad (2)$$

where the sum is over excited states $\langle K|$. X and Y denote the transition operators and ω represents the corresponding frequencies. $\hat{P}^{XY}$ is a permutation operator exchanging the operators X and Y. In this equation and throughout this paper, atomic units are used. For an exact-state formulation, eqn (1) and (2) are complex conjugate to each other.

Following ref. 12, these equations can be obtained as residues of the cubic response function:

$$-\lim_{\omega_Z+\omega_U\to\omega_J}(\omega_Z+\omega_U-\omega_J)\langle\langle X;Y,Z,U\rangle\rangle_{\omega_Y,\omega_Z,\omega_U} = \sum_{I,K}\hat{P}^{XY}\frac{\langle 0|X|I\rangle\langle I|Y|J\rangle\langle J|Z|K\rangle\langle K|U|0\rangle}{(\omega_X+\omega_I)(\omega_U-\omega_K)} \quad (3)$$

2.1 Two-photon absorption with coupled-cluster methods

In the following we adopt the above-mentioned approach to coupled-cluster response functions. The cubic response function in coupled-cluster theory is:[12,14]

$$\langle\langle X;Y,Z,U\rangle\rangle_{\omega_Y,\omega_Z,\omega_U} = \frac{1}{2}\hat{C}^{\pm\omega}\hat{P}^{XYZU}\left\{\frac{1}{4}\left(\eta^{ZU}+\frac{1}{2}\mathbf{F}t^{ZU}\right)t^{XY}+\frac{1}{4!}\mathbf{H}t^Xt^Yt^Zt^U + \frac{1}{6}\bar{t}^X\mathbf{C}t^Yt^Zt^U+\frac{1}{2}\bar{t}^X\mathbf{B}^Yt^Zt^U\right\} \quad (4)$$

where t^X is the first-order and t^{XY} is the second-order response of the cluster amplitudes. $\bar{t}^X$ is the first-order response of the corresponding Lagrangian multipliers, which are needed according to the $2n+1$-rule for the amplitudes and the $2n+2$-rule for the multipliers.[14,15] The operator $\hat{C}^{\pm}$ symmetrizes the equation with respect to a change in the sign of ω and complex conjugation. The remaining intermediates are defined in Table 1. For better readability, the frequency dependence of the response of the cluster amplitudes and Lagrangian multipliers has been omitted here. Details concerning the formation of the residue are published elsewhere.[12,14,16] The two-photon absorption matrix elements can be obtained as:[12]

$$M^{XY}_{J\leftarrow 0} = \hat{P}^{XY}(\tfrac{1}{2}\bar{E}^J\mathbf{B}t^Xt^Y + \bar{E}^J\mathbf{A}^Xt^Y) \quad (5)$$

$$M^{XY}_{0\leftarrow J} = \mathbf{G}t^Xt^YE^J + \hat{P}^{XY}(\mathbf{F}^Xt^YE^J + \bar{M}^J[\tfrac{1}{2}\mathbf{B}t^Xt^Y + \mathbf{A}^Xt^Y] + \bar{t}^X[\mathbf{B}t^Y + \mathbf{A}^Y]E^J) \quad (6)$$

Table 1 Matrices occurring in CC response functions.[12] The frequency dependencies of the response of the amplitudes and Lagrangian multipliers have been omitted for brevity. All matrices are derivatives of the coupled cluster Lagrangian L which is shown here for the CC2 method[8]

Term	Definition
η^{XY}	$\bar{\xi}^{XY} - \mathbf{F}t^{XY}$
ξ^X	$\left(\frac{\partial^2 L}{\partial X \partial \bar{t}}\right)_0$
ξ^{XY}	$\hat{P}^{XY}\{\frac{1}{2}\mathbf{B}t^Xt^Y + \mathbf{A}^Xt^Y\}_0$
$\bar{\xi}^{XY}$	$\mathbf{F}t^{XY} + \hat{P}^{XY}\{\frac{1}{2}\mathbf{G}t^Xt^Y + \mathbf{F}^Xt^Y + \bar{t}^Y\mathbf{B}t^X + \bar{t}^Y\mathbf{A}^X\}_0$
$\boldsymbol{F}_{\mu\nu}$	$\left(\frac{\partial^2 L}{\partial t_\mu \partial t_\nu}\right)_0$
$\boldsymbol{F}^X_{\mu\nu}$	$\left(\frac{\partial^3 L}{\partial t_\mu \partial t_\nu \partial X}\right)_0$
$\boldsymbol{G}_{\lambda\mu\nu}$	$\left(\frac{\partial^3 L}{\partial t_\lambda \partial t_\mu \partial t_\nu}\right)_0$
$\boldsymbol{H}_{\kappa\lambda\mu\nu}$	$\left(\frac{\partial^4 L}{\partial t_\kappa \partial t_\lambda \partial t_\mu \partial t_\nu}\right)_0$
$\boldsymbol{A}_{\mu\nu}$	$\left(\frac{\partial^2 L}{\partial \bar{t}_\mu \partial t_\nu}\right)_0$
$\boldsymbol{B}_{\lambda\mu\nu}$	$\left(\frac{\partial^3 L}{\partial \bar{t}_\lambda t_\mu \partial t_\nu}\right)_0$
$\boldsymbol{C}_{\kappa\lambda\nu\nu}$	$\left(\frac{\partial^4 L}{\partial \bar{t}_\kappa \partial t_\lambda \partial t_\mu \partial t_\nu}\right)_0$
L	$\langle HF\|\hat{\bar{H}} + [\hat{\bar{H}}, \hat{T}_2]\|HF\rangle + \sum_{\mu_1}\bar{t}_{\mu_1}\langle\mu_1\|\hat{\bar{H}} + [\hat{\bar{H}}, \hat{T}_2]\|HF\rangle + \sum_{\mu_2}\bar{t}_{\mu_2}\langle\mu_2\|\hat{\bar{H}} + [F, \hat{T}_2]\|HF\rangle$

where $\bar{E}^J$ and E^J are, respectively, the left and right eigenvectors of the Jacobi matrix $\mathbf{A}$ describing state J.

It is important to point out that in coupled-cluster theory $M^{XY}_{J\leftarrow 0}$ and $M^{XY}_{0\leftarrow J}$ are no longer complex conjugates to each other due to the non-Hermitian structure of the theory, so that both need to be calculated.

From the two-photon absorption matrix elements $M^{XY}_{J\leftarrow 0}$ and $M^{XY}_{0\leftarrow J}$, the transition rate for linearly polarized light can be obtained from[17]

$$S_{0J} = \frac{1}{15}\sum_{\mu\nu}(M^{\mu\mu}_{J\leftarrow 0}M^{\nu\nu}_{0\leftarrow J} + M^{\mu\nu}_{J\leftarrow 0}M^{\mu\nu}_{0\leftarrow J} + M^{\mu\nu}_{J\leftarrow 0}M^{\nu\mu}_{0\leftarrow J}), \quad (7)$$

where the summations μ and ν are over the components of the dipole operator.

From the transition rates, the two-photon absorption cross section in Göppert-Maier (GM) units is obtained as[17]

$$\sigma = \frac{16\pi^3\alpha a_0^5}{c}\frac{(\hbar\omega)^2}{\pi(\Gamma_f/2)}S_{0J}, \quad (8)$$

where α is the fine structure constant, c is the speed of light, ω is the photon energy (*i.e.* half the excitation energy in this work) and Γ_f is the damping constant which is chosen to be 0.5 eV according to ref. 18. In this definition $\hbar\cdot\omega$, Γ_f and S_{0J} are given in atomic units, and $a_0 = 5.291772108\cdot10^{-9}$ cm and $c = 2.99792458\cdot10^{10}$ cm s^{-1}.

2.2 The RI-CC2 approach and two-photon absorption

The RI-CC2 approach as implemented in TURBOMOLE has been widely used to calculate both excitation energies[9] and

 This journal is © the Owner Societies 2012

View Article Online

Published on 30 November 2011. Downloaded by Ruhr Universitat Bochum on 12/22/2018 1:15:42 PM.

first-order properties[19,20] of excited states. With the resolution-of-identity approximation, the demand for I/O and storage capacity is significantly reduced compared to other coupled-cluster implementations, making this approach an efficient tool to study molecules with up to 80 to 100 atoms using accurate basis sets. This also makes RI-CC2 the method of choice for calculating two-photon absorptions of larger molecules with a correlated wavefunction-based model.

The prominent feature of RI-CC2 is the use of the resolution-of-identity approximation to treat the 2-electron integrals,[9] reducing the calculation of the doubles cluster amplitudes to a few very efficient matrix–matrix multiplications:

$$\tilde{B}^{Q}_{ai} = \sum_{P} (ai\,\tilde{|}\,P) V^{-\frac{1}{2}}_{PQ}, \tag{9}$$

$$(ai\,\tilde{|}\,bj) \approx \sum_{PQ} (ai\,\tilde{|}\,P) V^{-1}_{PQ} (Q\,\tilde{|}\,bj) = \sum_{Q} \tilde{B}^{Q}_{ai} \tilde{B}^{Q}_{bj} \tag{10}$$

$$t^{ab}_{ij} = \frac{(ai\,\tilde{|}\,bj)}{\varepsilon_a - \varepsilon_i + \varepsilon_b - \varepsilon_j} \approx \frac{\sum_Q \tilde{B}^{Q}_{ai} \tilde{B}^{Q}_{bj}}{\varepsilon_a - \varepsilon_i + \varepsilon_b - \varepsilon_j}, \tag{11}$$

where V^{-1}_{PQ} is a two-index two-electron integral and $(ai\tilde{|}P)$ is a three-index two-electron integral in which a, b are indices of virtual and i, j are indices of occupied orbitals, respectively. P, Q are the indices of an auxiliary basis. For convenience, V^{-1}_{PQ} and $(ai\tilde{|}P)$ are contracted to $\tilde{B}^{Q}_{ai}$ intermediates. All these integrals refer to a Hamiltonian which is similarity transformed with the singles cluster amplitudes according to

$$\hat{\tilde{H}} = e^{-\hat{T}_1} \hat{H} e^{\hat{T}_1}. \tag{12}$$

By using the RI approximation, the storage of the doubles amplitudes t^{ab}_{ij} and other 4-index quantities can be completely avoided, which is essential for calculations with 1000 and more basis functions. Neither the ground-state doubles nor the doubles Lagrangian multipliers or responses of these are ever stored on disc. All doubles intermediates are calculated on-the-fly whenever needed and are immediately contracted to three- or two-index quantities which can easily be stored in memory or on disc.

For the implementation in the ricc2 module of TURBOMOLE, eqn (5) and (6) are first rewritten in a way that the contractions of the perturbed matrices $\mathbf{A}^X$ and $\mathbf{F}^X$ are expressed in terms of contractions of one-particle densities with perturbed one-electron integrals $\hat{h}^X$. We thus end up with the following expressions:

$$M^{XY}_{J\leftarrow 0} = \hat{P}^{XY}\{\tfrac{1}{2}\,\bar{E}^J\,\mathbf{B}t^X t^Y + D^A(\bar{E}^J, t^Y)\hat{h}^X\} \tag{13}$$

$$\begin{aligned} M^{XY}_{0\leftarrow J} = \hat{P}^{XY}\{&\tfrac{1}{2}\,\mathbf{G}t^X\,t^Y E^J + D^F(t^Y, E^J)\hat{h}^X + \tfrac{1}{2}\,\bar{M}^J\mathbf{B}t^X t^Y \\ &+ D^A(\bar{M}^J, t^Y)\hat{h}^X + \bar{t}^X\mathbf{B}t^Y E^J + D^A(\bar{t}^X, E^Y)\hat{h}^Y]\}. \end{aligned} \tag{14}$$

In these definitions, $\bar{M}^J$ denotes Lagrangian multipliers [12] for the state J.

While expressions for the density D^A are given in ref. 20, the density D^F is defined by

$$\begin{aligned} D^F_{pq} &= \sum_{\mu\nu} \frac{\partial \mathbf{F}^{\mathbf{X}}_{\mu\nu} t^Y_\mu E^J_\nu}{\partial h_{pq}}, \\ &= \sum_{\mu_1} \bar{t}_{\mu_1} \langle \mu_1 | [[\tau_{pq}, \tau_{\nu_1}], \tau_{\lambda_1}] | HF \rangle t^X E^J \\ &\quad + \sum_{\mu_2} \bar{t}_{\mu_2} \langle \mu_2 | [[\tau_{pq}, \tau_{\nu_2}], \tau_{\lambda_1}] | HF \rangle t^X E^J, \end{aligned} \tag{15}$$

where $\mathbf{F}$ is the matrix of second derivatives of the Lagrange function as defined in Table 1.

Similarly, the density D^A is defined *via* the derivatives of the Jacobian $\mathbf{A}^X$ with respect to the one-electron Hamiltonian integrals $\hat{h}^X_{pq}$. It is convenient to organize these densities in terms of blocks which are related to occupied and virtual orbitals. Working expressions for D^F and D^A can be found in Table 2. As can be seen from Table 2, both D^A and D^F contain contractions of two doubles vectors. These terms are denoted X and Y in Table 2. As soon as one of these vectors depends on a perturbation, this results in difficulties for the policy of not storing any N^4-intermediates, because the response of the doubles amplitudes and multipliers depends on the corresponding ground-state parameters. Consider for example the response of the doubles Lagrangian multipliers:

$$\bar{t}^X_{aibj} = \frac{\bar{\xi}^X_{aibj}}{\varepsilon_i - \varepsilon_a + \varepsilon_j - \varepsilon_b}, \tag{16}$$

$$\begin{aligned} \bar{\xi}^X_{aibj} &= \hat{P}^{ab}_{ij}(2 - \hat{P}_{ij})\left\{\bar{t}^{(0)}_{ai}\hat{F}^X_{jb} + \sum_Q \bar{\breve{B}}^Q_{ia}(\bar{t}^{(0)}, t^X) B^Q_{jb}\right\} \\ &\quad + \hat{P}^{ab}_{ij}\left\{\sum_e \bar{t}^{(0)}_{aiej}\hat{h}^X_{eb} - \sum_n \bar{t}^{(0)}_{aibn}\hat{h}^X_{jn}\right\}, \end{aligned} \tag{17}$$

where $\hat{h}^X_{pq}$ are the perturbed one-electron integrals and $\breve{B}^Q_{ia}$ are the integral intermediates as defined in Table 3. We can see that the second term of eqn (17), and thereby $\bar{t}^X_{aibj}$, depends on the ground-state doubles Lagrangian multipliers $\bar{t}^{(0)}_{aibj}$. These are obtained as

$$\bar{t}^{(0)}_{aibj} = \hat{P}^{ab}_{ij}(2 - \hat{P}_{ij}) \frac{\bar{t}^{(0)}_{ai}\hat{F}_{jb} + \sum_Q (B^Q_{ia} + \bar{\breve{B}}^Q_{ia}) B^Q_{jb}}{\varepsilon_i - \varepsilon_a + \varepsilon_j - \varepsilon_b}, \tag{18}$$

where $\hat{P}^{ab}_{ij}$ is a permutation operator which symmetrizes with respect to an exchange of pairs ai and bj while $\hat{P}_{ij}$ exchanges the indices i and j, *i.e.*

$$\hat{P}^{ab}_{ij} g_{aibj} = g_{aibj} + g_{bjai}, \tag{19}$$

$$\hat{P}_{ij} f_{ij} = f_{ji}. \tag{20}$$

Table 2 Density intermediates used in our implementation. $\bar{t}^{(0)}$ and $t^{(0)}$ denote the ground state Lagrangian multipliers or amplitudes, respectively. If R denotes doubles amplitudes (ground state or response) the 2 Cou-Exc-combination of R must be used: $\tilde{R} = 2R^{ab}_{ij} - R^{ab}_{ji}$

Term	Definition
$D^F_{ij}\,(t^X, E^J)$	0
$D^F_{ab}\,(t^X, E^J)$	0
$D^F_{ia}\,(t^X, E^J)$	$-\sum_c Y_{ac}(\bar{t}^{(0)}, t^X)E^J_{ci}$
	$-\sum_k X_{ik}(\bar{t}^{(0)}, t^X)E^J_{ak} - \sum_{bj}\bar{t}_{bj}R^X_{aj}E^J_{bi}$
$D^F_{ai}\,(t^X, E^J)$	0
$D^A_{ij}\,(L, R)$	$-\sum_a L_{aj}R_{ai} - X_{ij}(L,R)$
$D^A_{ab}\,(L, R)$	$\sum_i L_{ai}R_{bi} + Y_{ab}(L, R)$
$D^A_{ia}\,(L, R)$	$-\sum_c Y_{ac}\,(L, t^{(0)})R_{ci} - \sum_j X_{ij}(L, t^{(0)})R_{aj} - C_{ai}(L, R)$
$D^A_{ai}\,(L, R)$	0
$X_{ij}(L, R)$	$\sum_{abk} L^{ab}_{jk} R^{ab}_{ik}$
$Y_{ab}(L, R)$	$\sum_{cij} L^{ac}_{ij} R^{bc}_{ij}$
$C_{ai}(L, R)$	$\sum_{bj} L_{bj} R^{ab}_{ij}$

View Article Online

Published on 30 November 2011. Downloaded by Ruhr Universitat Bochum on 12/22/2018 1:15:42 PM.

Table 3 Definitions of intermediates used for the calculation of the response of the doubles Lagrangian multipliers using Laplace decomposition. x denotes a perturbation operator

Term	Definition
$k_{ai}^{x}(x)$	$x_{ai}e^{(\varepsilon_a-\varepsilon_i)t_\alpha}$
$\bar{k}_{ai}^{x}(x)$	$\sum_c \hat{h}_{ca}^{(1)}\, x_{ci}e^{(\varepsilon_c-\varepsilon_i)\ t_\alpha} - \sum_k x_{ak}e^{(\varepsilon_a-\varepsilon_k)\ t_\alpha}\, \hat{h}_{ik}^{(1)}$
$K_{ai}^{x,Q}(x)$	$x_{ai}^{Q}e^{(\varepsilon_a-\varepsilon_i)\ t_\alpha}$
$\bar{K}_{ai}^{x,Q}(x)$	$\sum_c \hat{h}_{ca}^{(1)}\, x_{ci}^{Q}e^{(\varepsilon_c-\varepsilon_i)\ t_\alpha} - \sum_k x_{ak}^{Q}\, e^{(\varepsilon_a-\varepsilon_k)\ t_\alpha}\, \hat{h}_{ik}^{(1)}$
$\breve{B}_{ia}^{Q}$	$\sum_c \bar{t}_{ci}\hat{B}_{ca}^{Q} - \sum_k \bar{t}_{ak}\hat{B}_{ik}^{Q}$

If a contraction with a third four-index quantity (*e.g.* right doubles eigenvectors) has to be calculated, this would require either storage of at least one N^4-intermediate or a decomposition of the integrals or the denominators in the definition of the doubles vector. Pedersen *et al.*[21] reported an implementation of the CC2 linear response function where a Cholesky decomposition of the integrals was used for this purpose. We decided to use instead a numerical Laplace transformation which can be implemented efficiently without precomputing and storing $\bar{t}^{(0)}$ since

$$\frac{1}{\varepsilon_i-\varepsilon_a+\varepsilon_j-\varepsilon_b} = \int_0^\infty e^{-(\varepsilon_i-\varepsilon_a+\varepsilon_j-\varepsilon_b)t}\mathrm{d}t, \approx \sum_\alpha \omega_\alpha e^{-(\varepsilon_i-\varepsilon_a+\varepsilon_j-\varepsilon_b)t_\alpha}, \tag{21}$$

with sampling points t_α and weights ω_α.

We can rewrite the last two terms of eqn (17) by inserting eqn (18) and (21) and the definitions from Table 3, leading to

$$\sum_c \hat{h}_{cb}^{(1)}\bar{t}_{aicj}^{(0)} - \sum_k \bar{t}_{aibk}^{(0)}\hat{h}_{jk}^{(1)} \approx \hat{P}_{ij}^{ab}(2-\hat{P}_{ij})\sum_\alpha \omega_\alpha\left\{k_{ai}^{\alpha}(\bar{t}^{(0)})\bar{k}_{bj}^{\alpha}(\hat{F}) + \sum_Q K_{ai}^{\alpha,Q}(B+\breve{B})\bar{K}_{bj}^{\alpha,Q}(B)\right\}. \tag{22}$$

All $O(N^4)$ scaling steps for the computation of $\bar{k}$ and $\bar{K}$ can be done as efficient matrix–matrix multiplications.

3 Computational details

The structures of *p*-nitroaniline, *p*-nitroaminostilbene and *p*-aminonitrophenylvinylstilbene were optimized at the MP2 level of theory using the ricc2 module of the TURBOMOLE program package. In order to allow for a more direct comparison with previous DFT literature data,[22] *p*-nitroaniline was calculated using the aug-cc-pVDZ[23] basis, whereas for *p*-aminonitrostilbene and *p*-aminonitrophenylvinylstilbene, the cc-pVDZ[23] basis was used. For the AF240 dye molecule we used a geometry which was optimized at the DFT level with the B3LYP exchange–correlation functional and the 6-31G* basis[24,25] in order to obtain results that are more directly comparable to the results obtained in ref. 22. The comparison with DFT results is to some part based on a comparison with previous literature data for two-photon absorption (TPA) cross sections, but we also complemented these results by additional TD-DFT calculations using the CAM-B3LYP,[10] B3LYP[26–31] and BP86-functionals.[28,29,32]

The substituted azobenzene derivatives (*p*-aminonitroazobenzene, *p*-aminoazobenzene and *p*-diaminoazobenzene) were optimized using the 6-311++G** basis[33] and the MP2 method in order to allow for a direct comparison with results of Silva *et al.*[18]

For all molecules, the same basis set was used for the calculation of the TPA cross sections at the coupled-cluster and the density functional level of theory as were used to optimize the molecular structures. All coupled-cluster calculations have been done with a development version of the TURBOMOLE program package[34] and employed the frozen core approximation, whereas all DFT calculations presented here have been performed with the Dalton quantum chemistry package.[35]

The molecular tweezer complex presented in Section. 4.4 was studied in the cc-pVDZ basis using a geometry based on a B3LYP-optimization.

3.1 Laplace error

To investigate the error caused by the numerical Laplace transformation of the orbital energy denominators we performed several calculations on naphthacene and thiophene.

The Laplace sampling points t_α and weights ω_α are obtained by minimizing the Laplace error function $F^{\mathrm{Lap}}(t_\alpha)$ for a number of sampling points n:[36]

$$F^{\mathrm{Lap}}(t_\alpha) = \int_{\varepsilon_{\min}}^{\varepsilon_{\max}} \left(\frac{1}{\varepsilon_{aibj}} - \sum_\alpha^n \omega_\alpha e^{-\varepsilon_{aibj}t_\alpha}\right), \tag{23}$$

$$\varepsilon_{aibj} = \varepsilon_a - \varepsilon_i + \varepsilon_b - \varepsilon_j \tag{24}$$

In the calculations, the error of the biggest $M_{0\leftarrow J}^{\mu\nu}$ transition matrix elements for each of the studied systems was evaluated both with respect to the value of the Laplace error function (which depends on the number of sampling points) and the threshold for the convergence of the linear equation systems for the response vectors $\bar{t}$, $\bar{t}^X$, $\bar{M}^J$ and t^X.

All calculations were performed using the aug-cc-pVTZ basis set,[23,37] and the corresponding auxiliary basis set.[38]

For studying the Laplace error we first performed a reference calculation with 18 sampling points and a convergence limit of 10^{-10}. We then varied the number of sampling points and the convergence threshold for the linear equation systems.

In this study it was found that the error in $M_{0\leftarrow J}^{\mu\nu}$ is significantly higher than the error in $M_{J\leftarrow 0}^{\mu\nu}$ since the latter only contains one term which is affected by the Laplace transformation, while in the former several terms on the one hand depend on the Laplace transformation and on the other hand one term also depends on both the response of the amplitudes and the Lagrangian multipliers. For this reason, we will in the following only consider the error in $M_{0\leftarrow J}^{\mu\nu}$ since the error in $M_{J\leftarrow 0}^{\mu\nu}$ was found to be much smaller.

The results are shown in Fig. 1 for the 2 ^1A_g state of naphthacene. The 2 ^1A_g state was selected because of its remarkably high TPA. Fig. 2 shows the results for the 2 $^1B_2$-state of thiophene. Thiophene in general, and the 2 $^1B_2$-state in particular, were selected in order to study a system which differs chemically from naphthacene due to the sulfur atom which plays an important role for the excitation into the 2 $^1B_2$ state.

 This journal is © the Owner Societies 2012

View Article Online

Published on 30 November 2011. Downloaded by Ruhr Universitat Bochum on 12/22/2018 1:15:42 PM.

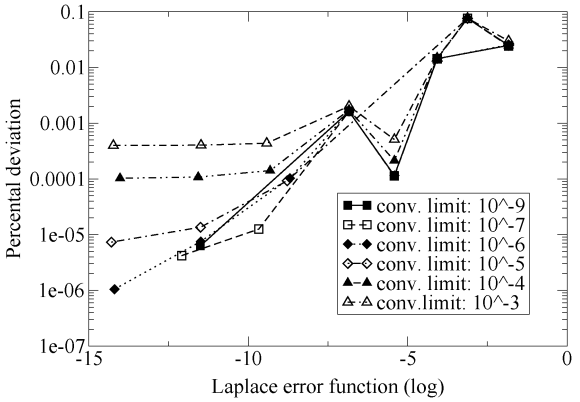


Fig. 1 Laplace error for TPA of the 2 ^1A_g state of naphthacene. T_{LRE} is the convergence threshold for the linear equation systems and Δ is the relative error.

In the regime where the convergence threshold for the linear response equations (T_{LRE}) is tight compared to the square root of the Laplace error function, the plots show an approximately linear relation between the relative errors in the transition matrix elements. The local minimum in the plot for naphthacene at $\sqrt{F^{\mathrm{Lap}}} = 1.9 \times 10^{-3}$ is caused by a change of sign in the relative error.

For more loose convergence thresholds T_{LRE} we reach a turning point beyond which the accuracy is limited by the convergence threshold of the response equations. We found that the relative errors in the largest transition moments are bound by

$$\Delta = 0.5 \cdot (T_{\mathrm{LRE}} + \sqrt{F^{\mathrm{Lap}}}). \qquad (25)$$

This relation can be used in production calculations to adapt the threshold for F^{Lap} automatically to the requested accuracy.

It is noteworthy that already with very loose values of $F^{\mathrm{Lap}} \approx 10^{-1}$, the errors in the two-photon transition moments $M^{XY}_{0\leftarrow J}$ are less than 1% and the errors in $M^{XY}_{J\leftarrow 0}$ are even smaller. For many practical applications, this level of numerical accuracy will be more than sufficient. $F^{\mathrm{Lap}} \approx 10^{-1}$ requires typically only 2–3 grid points, making the numerical Laplace transformation of the denominators an efficient tool for avoiding storage bottlenecks due to the response of doubles quantities in RI-CC2 higher-order response calculations.

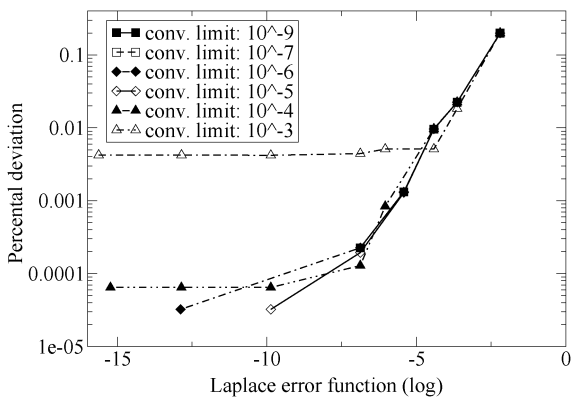


Fig. 2 Laplace error for the 2 $^1B_2$-state of thiophene plotted as a function of the threshold for the solution of the linear equation systems. T_{LRE} is the convergence threshold for the linear equation systems and Δ is the relative error. The series for $_{\mathrm{LRE}}$ 10^{-7} is cut off since the deviation to the reference is zero at small values for the error function.

4 Results and discussion

In this section we present the results of our calculations on some larger molecules that have previously been studied by CAM-B3LYP.

We are in particular interested in charge-transfer states, because TD-DFT is known to experience problems in treating these states correctly.[39] Significant improvements in the description of excited states were achieved with the introduction of the CAM-B3LYP functional,[10] and one goal of this study is to benchmark these improvements with a correlated wavefunction-based method for larger molecules in order to complement earlier benchmark studies.[11,40]

For this comparison we have chosen a set of substituted benzene derivatives which were partially investigated in ref. 22, as well as a set of substituted azobenzene derivatives from ref. 18. As large-scale applications of RI-CC2, we chose the AF240 dye molecule which was studied in ref. 22 and a so-called "molecular tweezer complex" based on a structure from ref. 41.

4.1 Substituted benzene derivatives

To compare the results of TD-DFT and CC2 we did a series of calculations on a set of "push–pull"-substituted benzene derivatives, which consisted of *p*-nitroaniline, *p*-aminonitrostilbene and a compound we call *p*-aminonitrophenylvinylstilbene. While for the former compounds, reference data are found in ref. 22, no data are yet available for the latter. However, since it is a higher homologue of *p*-aminonitrostilbene, we did calculations both with TD-DFT and CC2 and found that this molecule has quite high two-photon absorption cross sections. *p*-Aminonitrophenylvinylstilbene was studied in an all-*trans* conformation. In this conformation resulting from a MP2 geometry optimization, the three aromatic rings do not form one plane, being instead slightly twisted towards each other. The structures of the studied molecules are shown in Fig. 3 and 6.

For all molecules, we report results for the 10 lowest singlet states (although we calculated more states in order to ensure that the lowest states are found) and identify states that have a strong charge transfer (CT) character.

In general, the ordering of the states obtained with CC2 and CAM-B3LYP is in good agreement. With the B3LYP functional, the deviations in the ordering are notably larger and with BP86, even some lower-lying states could not be assigned to the states found with CC2.

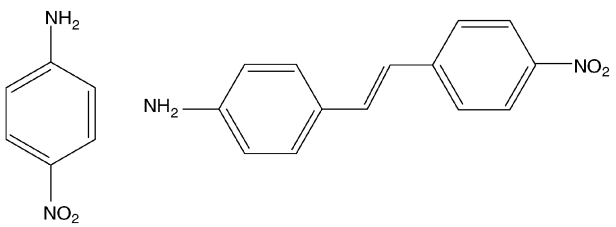


Fig. 3 Structures of *p*-nitroaniline and *p*,*p*-4,4′-nitroaminostilbene.

View Article Online

Published on 30 November 2011. Downloaded by Ruhr Universitat Bochum on 12/22/2018 1:15:42 PM.

Table 4 TPA cross sections (σ) and excitation energies for *p*-nitroaniline. The order of states follows the order found in CC2. The corresponding state index found in the TD-DFT calculations is given in the column "state no."

CC2				CAM-B3LYP			B3LYP			BP86		
State no.	Energy/eV	σ/GM	State character	State no.	Energy/eV	σ/GM	State No.	Energy/eV	σ/GM	State no.	Energy/eV	σ/GM
1	3.95	0.0		1	3.97	0.0	1	3.83	0.0	2	3.53	0.00
2	4.52	57		2	4.38	106	2	3.92	99	1	3.50	73
3	4.54	1		3	4.43	0.3	3	4.31	0.0	4	4.06	0.0
4	4.64	0.0		4	4.74	0.1	5	4.97	0.0	5	4.54	0.1
5	5.25	3	CT	6	5.48	10	6	5.10	11	15	5.87	4.9
6	5.66	0.2		5	5.47	0.4	4	4.38	0.1	3	3.98	0.00
7	6.05	0.1	CT	8	6.29	0.4	7	5.87	0.5			
8	6.1	7		10	6.45	1	10	6.01	17			
9	6.31	0.0	CT	9	6.32	0.6	9	6.00	0.1	11	5.50	0.0
10	6.34	45		7	6.20	94	8	5.89	57			

Table 5 TPA cross sections (σ) and excitation energies for *p*-aminonitrostilbene. The order of states follows the order found in CC2. The corresponding state index found in the TD-DFT calculations is given in the column "state no."

CC2				CAM-B3LYP			B3LYP			BP86		
State no.	Energy/eV	σ/GM	State character	State No.	Energy/eV	σ/GM	State No.	Energy/eV	σ/GM	State no.	Energy/eV	σ/GM
1	3.73	430		1	3.55	858	1	2.95	1308	1	2.43	1022
2	4.00	0.0	CT	2	3.93	0.0	2	3.73	0.0	2	3.2	0.0
3	4.52	26	CT	4	4.62	205	9	4.61	18	9	4.01	6
4	4.59	0.0	CT	3	4.42	0.0	5	4.24	0.0	6	3.76	0.0
5	4.64	12	CT	5	4.67	8.3	4	4.20	319			
6	5.12	31		6	4.92	705	3	4.04	987	3	3.5	178
7	5.44	3257		7	5.21	7059	7	4.37	271	7	3.78	19
8	5.64	254	CT	8	5.45	842	8	4.55	26	5	3.64	4.5
9	5.78	41	CT	9	5.66	41	6	4.26	303	4	3.59	0.2
10	6.29	6		10	6.06	22	10	5.29	81			

Table 6 TPA cross sections (σ) and excitation energies for *p*-aminonitrophenylvinylstilbene. The order of states follows the order found in CC2. The corresponding state index found in the TD-DFT calculations is given in the column "state no."

CC2				CAM-B3LYP			B3LYP			BP86		
State no.	Energy/eV	σ/GM	State character	State no.	Energy/eV	σ/GM	State No.	Energy/eV	σ/GM	State No.	Energy/eV	σ/GM
1	3.50	820		1	3.31	1802	1	2.51	5708	1	1.82	5353
2	4.00	0.4	CT	2	3.92	0.0	4	3.73	1	4	3.16	2
3	4.38	26		3	4.20	395	3	3.48	324	2	2.75	1654
4	4.44	109		6	4.59	3499	5	4.01	5			
5	4.52	18	CT	4	4.34	1	8	4.15	335			
6	4.53	182		7	4.63	1247						
7	4.62	44.5		8	4.64	742	10	4.29	1			
8	4.73	6791		5	4.53	18 276	2	3.33	3967	3	2.78	134
9	5.23	430		9	5.04	142	7	4.11	694			
10	5.57	14		10	5.37	1836	6	4.04	294	5	3.22	82

The results of the calculations are displayed in Tables 4–6 for *p*-nitroaniline, *p*-aminonitrostilbene and *p*-aminonitrophenylvinylstilbene, respectively. In Tables 4, 5 and 7, comparisons of the two-photon absorption cross sections for linear polarized light obtained from CC2 and TD-DFT with the CAM-B3LYP, B3LYP and BP86 functionals are shown for the three molecules. The TPA values are plotted in Fig. 4, 5 and 7.

For *p*-aminonitrostilbene, both excitation energies and the relations between the TPA values for the first three states are in good agreement with the findings of Rudberg *et al.*[22]

Overall, TD-DFT and CC2 are in good agreement in reproducing the lowest inactive states which are S_1 in *p*-nitroaniline and S_2 and S_4 in *p*-aminonitrostilbene and S_2 in *p*-aminonitrophenylvinylstilbene, respectively. For the first TPA-active states,

Table 7 TPA cross sections (σ) and excitation energies for *p*-aminonitroazobenzene

CC2				CAM-B3LYP[18]			Experiment[42]	
State no.	Energy/eV	σ/GM	Character	State No.	Energy/eV	σ/GM	Energy/eV	σ/GM
1	2.81	0.0	$n \rightarrow \pi^*$	1	2.82	0.3		
2	3.35	350	$\pi \rightarrow \pi^*$	2	3.47	29	2.53	100
4	4.4	33	$\pi \rightarrow \pi^*$	3	4.74	39	3.6	400
6	4.5	18	$\pi \rightarrow \pi^*$					

CC2 and the three density functionals are in reasonable agreement, with CC2 always yielding the lowest TPA cross section. This is a tendency that is also seen for most of the

 This journal is © the Owner Societies 2012

View Article Online

Published on 30 November 2011. Downloaded by Ruhr Universitat Bochum on 12/22/2018 1:15:42 PM.

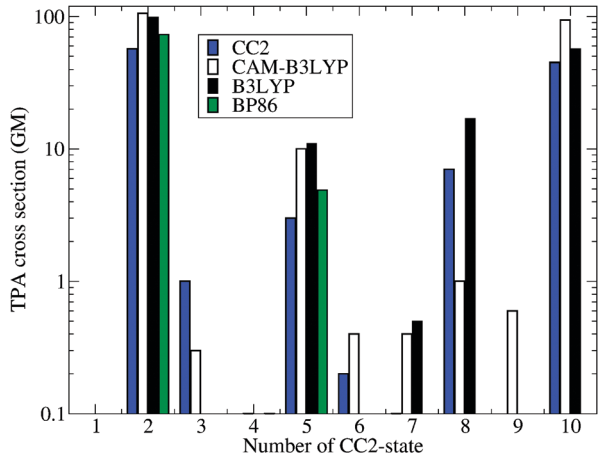


Fig. 4 Comparison of the linear component of TPA transition rates in *p*-nitroaniline.

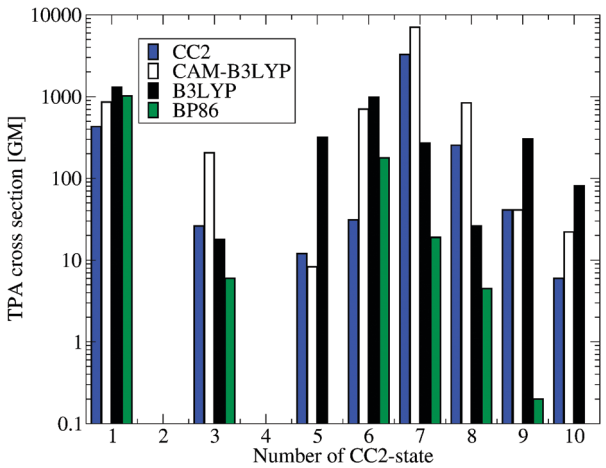


Fig. 5 Comparison of the linear component of TPA transition rates in *p*-aminonitrostilbene.

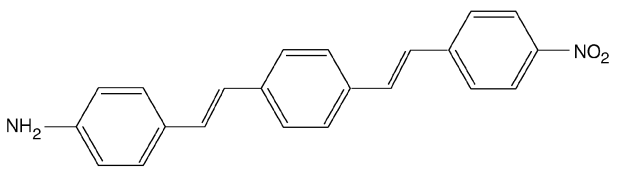


Fig. 6 Structure of *p*-aminonitrophenylstilbene.

other states with a rather high TPA activity, where the transition rate from CAM-B3LYP is normally higher than the one from CC2. For the B3LYP and BP86 values, such tendencies are not observed.

A prominent exception from these trends is the second TPA active state in all three molecules, exhibiting a major disagreement between the CC2 and TD-DFT results. In *p*-aminonitrostilbene, this state (S_3) is of CT character.

For BP86, only a very small number of states could be assigned to the CC2 states and the results also show very little agreement with those obtained from CAM-B3LYP and B3LYP.

On the whole, for the substituted benzene derivatives we find that there is a tendency for the CAM-B3LYP TPA cross sections for being higher than the CC2 values, and only very few states display a deviation from this general rule. Whereas the BP86 and B3LYP results appear to be quite unreliable, CC2 and CAM-B3LYP show in most cases at least a qualitative agreement. These observations are in line with the results for some small molecules in ref. 11.

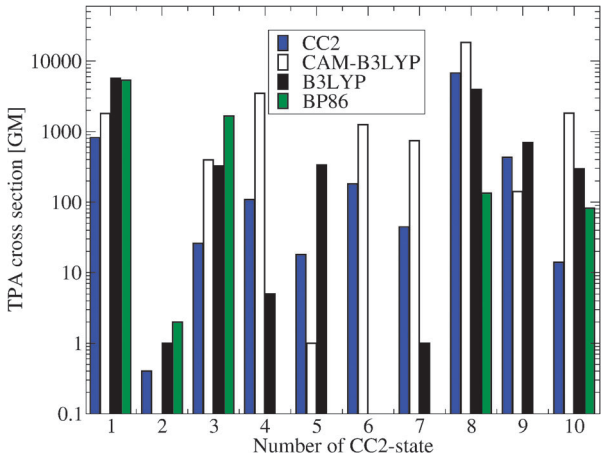


Fig. 7 Comparison of the linear component of TPA transition rates in *p*-aminonitrophenylvinylstilbene.

4.2 Substituted azobenzene derivatives

The series of substituted azobenzene derivatives we present here (Fig. 8) was studied with CAM-B3LYP by Silva *et al.*,[18] who reported not only TPA data and excitation energies but also assigned the reported states to be of $\pi \rightarrow \pi^*$ or $n \rightarrow \pi^*$ character, making it easier to assign the CC2 results to the CAM-B3LYP ones. The calculated CC2 as well as CAM-B3LYP values[18] and experimental results[42] for *p*-aminonitroazobenzene (*p*ANA), *p*-aminoazobenzene (*p*AAB) and *p*-diaminoazobenzene (*p*DAA) are listed in Tables 7–9, respectively. Experimental data were obtained from measurements in DMSO.

In ref. 18, the lowest-lying state is described to be dominated by an $n \rightarrow \pi^*$-transition for all three molecules. This, and the fact that the TPA cross sections are small for this transition in all three molecules, is fully reproduced by the CC2 calculations. Although the S_1 state in *p*ANA is dark in both the CC2 and CAM-B3LYP calculations, in experiment a state with a similar excitation energy is found which exhibits a cross section of 100 GM. Silva *et al.* assign this state to correspond to the S_3 state from CAM-B3LYP, although the difference in excitation energy is as large as 0.89 eV, whereas the energy difference to the S_2 state is only 0.41 eV for CAM-B3LYP and 0.42 eV for CC2, respectively.

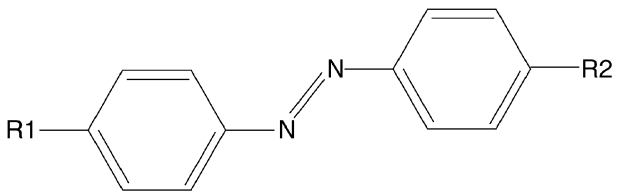


Fig. 8 Structure of the azobenzene derivatives that were studied: R1 = R2 = NH_2: *p*,*p*-diaminoazobenzene; R1 = H, R2 = NH_2: *p*-aminoazobenzene; R1 = NO_2, R2 = NH_2: 4,4′-nitroaminoazobenzene.

View Article Online

Published on 30 November 2011. Downloaded by Ruhr Universitat Bochum on 12/22/2018 1:15:42 PM.

Table 8 TPA cross sections (σ) and excitation energies for *p*-aminoazobenzene

CC2				CAM-B3LYP[18]			Experiment[42]	
State no.	Energy/ eV	σ/ GM	Character	State No.	Energy/ eV	σ/ GM	Energy/ eV	σ/ GM
1	2.92	0.0	n → π*	1	2.89	0.01		
2	3.67	131	π → π*	2	3.68	6		
3	4.48	8.7	π → π*	3	4.95	128	4.09	100

Table 9 TPA cross sections (σ) and excitation energies for *p*-diaminoazobenzene

CC2				CAM-B3LYP[18]			Experiment[42]	
State no.	Energy/ eV	σ/ GM	Character	State no.	Energy/ eV	σ/ GM	Energy/ eV	σ/ GM
1^1B	3.00	0.0	n → π*	1	2.93			
2^1B	3.52	0.1	π → π*	2	3.50			
1^1A	4.4	646	π → π*	3	4.54	25	4.09	400
2^1A	4.54	872	π → π*					

In ref. 18, S_2 always corresponds to π → π*-transitions. This can in all cases be reproduced in CC2 although the involved orbitals vary. In *p*ANA, the second state is dominated by the HOMO–LUMO transition.

For the CC2 calculations on *p*ANA and *p*AAB, S_2 shows a TPA cross section which is much higher than the one of the second state in CAM-B3LYP, but both the excitation energies and the TPA cross sections nevertheless fit quite well—and even better than CAM-B3LYP—to the experimental values in ref. 42 that have been assigned to the S_3 state of the CAM-B3LYP study in ref. 18.

In *p*DAA, the S_2 state from the CC2 calculation fits well with CAM-B3LYP both for the excitation energy and its (nearly zero) TPA cross section. Additionally, we found two states (1^1A and 2^1A) that match fairly well with the experiment both in terms of the excitation energies and TPA cross sections while the cross section predicted by CAM-B3LYP for the S_3 state disagrees with both experimental and CC2 results.

Among the CC2 results for *p*ANA, we found S_4 and S_6 to be of π → π* character and to fit to the S_3 state from CAM-B3LYP both in excitation energy and TPA cross section. However, experimental data for these states are not available.

In the case of *p*AAB, the S_3 state found in the CC2 calculation, which is nearly dark, fits quite well to the S_2 state found with CAM-B3LYP concerning the TPA cross sections, although the excitation energies deviate significantly.

On the whole, although some irregularities in the state ordering were found, the CC2 results fit reasonably well to both the experimental and CAM-B3LYP values.

4.3 AF240

The AF240 dye molecule (Fig. 9) has been studied earlier both experimentally[43] and theoretically.[22] We did TPA calculations both with CC2 and CAM-B3LYP for, respectively, the 20 and 15 lowest singlet states. The results of the CC2 calculations for the first five states and the assignment of the calculated CAM-B3LYP-states are given in Table 10.

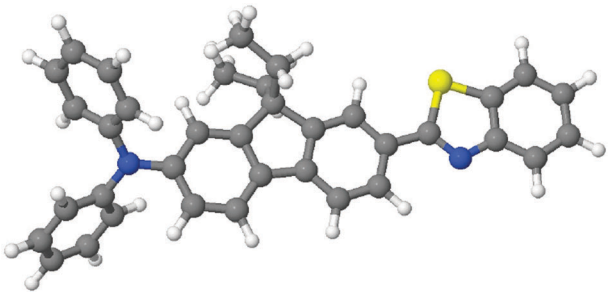


Fig. 9 Structure of AF240.

Table 10 TPA cross sections (σ) and excitation energies for the five lowest states of AF240 calculated with CC2 and CAM-B3LYP

CC2			CAM-B3LYP	
Energy/eV	σ/GM	State character	Energy/eV	σ/GM
3.45	618		3.59	736
4.12	6.5		4.36	8.5
4.34	183	CT	4.42	852
4.47	65	CT	4.55	117
4.48	47	CT	4.66	73

The four lowest excitation energies of our CAM-B3LYP calculations are in agreement with the values from ref. 22.

The results for the S_1 and S_2 states agree well between CC2 and CAM-B3LYP both for the ordering and the excitation energies, and for the TPA cross sections. These states have the character of valence excitations. To visualize our results, in Fig. 10 we plotted a simulated spectrum of AF240 containing both the five lowest CC2 and CAM-B3LYP states and their TPA cross sections. These spectra were plotted by centering Gaussians at the excitation energies. These Gaussians have unit width and their heights correspond to the TPA cross section. As can be seen from the spectrum, the two lowest excitations are in very good agreement both in intensity and in their shift. However the S_3 state from CAM-B3LYP has a very high absorption peak which cannot be reproduced by CC2, whereas the other peaks are in quite good agreement if a slight blue-shift of all CAM-B3LYP results is assumed. We note that the peak at 550 nm from the CC2 calculation contains two states which are very close in energy.

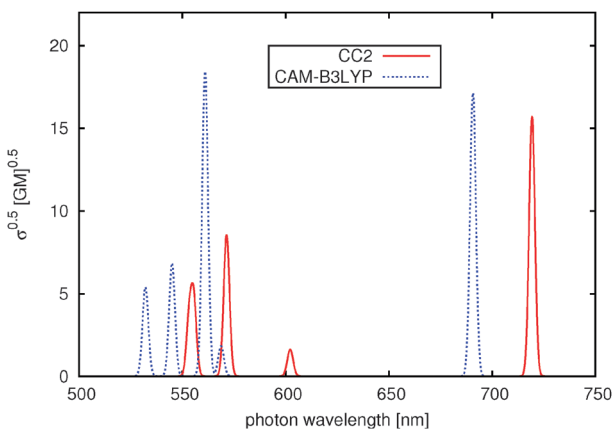


Fig. 10 Simulated TPA spectrum of AF240.

This journal is © the Owner Societies 2012

View Article Online

Published on 30 November 2011. Downloaded by Ruhr Universitat Bochum on 12/22/2018 1:15:42 PM.

4.4 Molecular tweezer complex

To study in detail the behavior of the CC2 implementation in treating two-photon absorptions with strong charge transfer in weakly bound systems, a molecular tweezer complex was studied, motivated by the work of Chakrabarti and Ruud.[41] For this original complex, built from 4,6-bis-(6-acrid-9-yl)-pyridin-2-yl-pyrimidine encapsulating a trinitrofluorinone (TNF) molecule through weak intermolecular interactions, Chakrabarti and Ruud reported the largest TPA cross section to date through CAM-B3LYP density functional theory calculations.[41,44] The large TPA cross sections were shown to arise from an intermolecular charge-transfer state which is not present in the isolated fragments that constitute the complex.

To make the system feasible for our method, we had to reduce the size of the tweezer complex compared to that originally used by Chakrabarti and Ruud.[41] This was achieved by removing one fused aromatic ring from both arms of the tweezer complex and a fused aromatic ring from the central TNF molecule in the original structure. The resulting binding sites of the carbon atoms were saturated with hydrogen using a bond length of 0.95 Å on the tweezer and 1.09 Å on the central molecule, and the structure was used without further optimization. The structure of the complex is shown in Fig. 11. This is the largest molecule which has ever been studied concerning TPA using a coupled-cluster method.

We calculated excitation energies for the 12 lowest singlet states in CC2 and for the 15 lowest singlet states in CAM-B3LYP, even though we performed TPA calculations only for the resulting five lowest states. The results for both CC2 and CAM-B3LYP are listed in Table 11 and illustrated in Fig. 12.

For both methods, the lowest excitation was from quite deep-lying orbitals to the LUMO with all major contributing orbitals being located on the TNF fragment. In CC2, we also find that the S_3 and S_4 states are dominated by excitations from quite low-lying orbitals, whereas the S_2 and S_5 states correspond well with the S_2 and S_3 states obtained in the CAM-B3LYP calculations. These latter states, found both in the CC2 and CAM-B3LYP calculations, do have large contributions from the HOMO–LUMO transition, in both cases exhibiting large intermolecular charge transfer between one arm of the tweezer (HOMO) to the TNF molecule (LUMO).

Despite the differences observed between CC2 and CAM-B3LYP, there is a qualitative agreement between the CC2 and CAM-B3LYP results for all states that could be assigned. This verifies that the CAM-B3LYP functional is indeed capable of rather accurately describing intermolecular charge-transfer excitations. Although this modified model system for the tweezer complex does not show the extraordinarily high two-photon cross sections observed in ref. 41, it gives strong support for the findings in that work, as there is no reason to assume that a CC2 calculation on the full tweezer complex, if computationally feasible, would not corroborate the earlier CAM-B3LYP calculations.

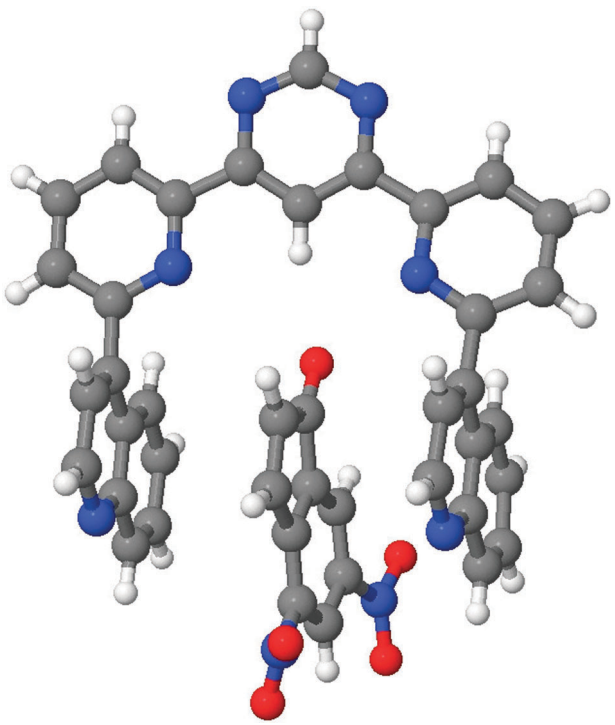


Fig. 11 Structure of the modified molecular tweezer complex.

Table 11 TPA cross sections σ, excitation energies and one-photon oscillator strengths f_{1PA} for the molecular tweezer complex. The ordering of the states follows the order found in CC2 with the corresponding number in TD-DFT given in the column labeled "state no."

CC2					CAM-B3LYP		
State no.	Energy / eV	σ^2/ GM	f_{1PA}/a.u.	State character	State no.	Energy/ eV	σ/ GM
1	2.97	0.9	1.7×10^{-4}		1	3.15	1.0
2	3.61	39.6	1.8×10^{-2}		2	3.25	72.8
3	3.8	3.0	1.6×10^{-3}				
4	3.81	45.5	1.2×10^{-2}				
5	3.93	341.0	2.6×10^{-3}	CT	3	3.63	165.9

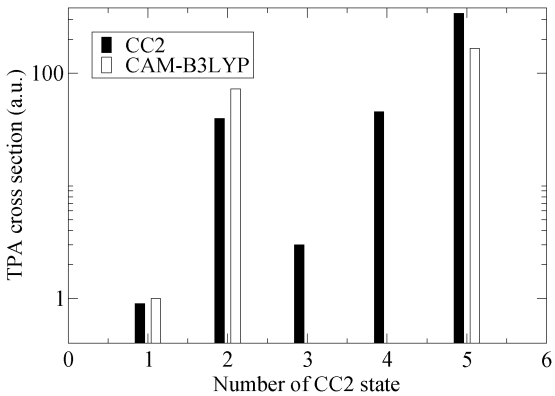


Fig. 12 Comparison of the linear component of TPA transition rates in a molecular tweezer complex.

5 Summary and outlook

An implementation of two-photon absorption matrix elements for CC2 using the RI approximation for the electron repulsion integrals has been presented. To avoid storage of large arrays, we introduced a numerical Laplace transformation of the coupled-cluster ground-state amplitudes and Lagrangian multipliers.

View Article Online

Published on 30 November 2011. Downloaded by Ruhr Universitat Bochum on 12/22/2018 1:15:42 PM.

This approximation was shown to introduce errors well below 1% already with only few grid points.

In a series of test calculations, we focused on a comparison of the CC2 results with results from TD-DFT with different functionals. In these calculations, CC2 served as a benchmark for TD-DFT because it is well known that TD-DFT has difficulties in treating CT transitions. For the CAM-B3LYP functional, we could not find fundamental disagreements between the results for CT- and non-CT states, whereas the B3LYP and BP86 functionals were shown to give significantly poorer results. In this sense, we can regard this as a strong indication of the reliability of the CAM-B3LYP functional.

In addition, we demonstrated that our implementation is capable of treating molecules with more than 70 atoms. As a consequence, we have reported TPA cross sections for the largest molecule that has ever been treated for this property by a coupled-cluster method. Our CC2 implementation has thus enabled a wavefunction-based alternative for TPA calculations on chromophores which appear as building blocks in many molecules which are of relevance in practical TPA applications.

Acknowledgements

D.H.F would like to acknowledge the support of Studienstiftung des Deutschen Volkes through a PhD scholarship as well as financial support from the Center for Computational and Theoretical Chemistry (CTCC) at the University of Tromsø and the graduate school of SFB 558. D.H.F. and C.H. acknowledge financial support by the Deutsche Forschungsgemeinschaft through grant HA 2588/5-1. K.R. was supported by the Norwegian research council through a center of excellence grant (Grant No. 179568/V30).

References

1 M. Göppert-Mayer, *Ann. Phys. (Berlin, Ger.)*, 1931, **401**, 273–294.
2 W. Kaiser and C. G. B. Garrett, *Phys. Rev. Lett.*, 1961, **7**, 229–231.
3 J. D. Bhawalkar, G. S. He and P. N. Prasad, *Rep. Prog. Phys.*, 1996, **59**, 1041.
4 A. Dreuw and M. Head-Gordon, *Chem. Rev.*, 2005, **105**, 4009–4037.
5 D. J. Tozer, R. D. Amos, N. C. Handy, B. O. Roos and L. Serrano-Andres, *Mol. Phys.*, 1999, **97**, 859–868.
6 A. Dreuw, G. R. Fleming and M. Head-Gordon, *Phys. Chem. Chem. Phys.*, 2003, **5**, 3247–3256.
7 A. Dreuw, J. L. Weisman and M. Head-Gordon, *J. Chem. Phys.*, 2003, **119**, 2943–2946.
8 O. Christiansen, H. Koch and P. Jørgensen, *Chem. Phys. Lett.*, 1995, **243**, 409–418.
9 C. Hättig and F. Weigend, *J. Chem. Phys.*, 2000, **113**, 5154–5161.
10 T. Yanai, D. P. Tew and N. C. Handy, *Chem. Phys. Lett.*, 2004, **393**, 51–57.
11 M. J. Paterson, O. Christiansen, F. Pawlowski, P. Jørgensen, C. Hättig, T. Helgaker and P. Sałek, *J. Chem. Phys.*, 2006, **124**, 054322.
12 C. Hättig, O. Christiansen and P. Jørgensen, *J. Chem. Phys.*, 1998, **108**, 8331–8354.
13 H. Koch and P. Jørgensen, *J. Chem. Phys.*, 1990, **93**, 3333–3344.
14 O. Christiansen, P. Jørgensen and C. Hättig, *Int. J. Quantum Chem.*, 1998, **68**, 1–52.
15 T. Helgaker and P. Jørgensen, *Adv. Quantum Chem.*, 1988, **19**, 183–245.
16 J. Olsen and P. Jørgensen, *J. Chem. Phys.*, 1985, **82**, 3235–3264.
17 R. R. Birge and B. M. Pierce, *J. Chem. Phys.*, 1979, **70**, 165–178.
18 D. L. Silva, P. Krawczyk, W. Bartkowiak and C. R. Mendonça, *J. Chem. Phys.*, 2009, **131**, 244516.
19 A. Köhn and C. Hättig, *J. Chem. Phys.*, 2003, **119**, 5021–5036.
20 C. Hättig and A. Köhn, *J. Chem. Phys.*, 2002, **117**, 6939–6951.
21 T. B. Pedersen, A. M. J. S. de Merás and H. Koch, *J. Chem. Phys.*, 2004, **120**, 8887–8897.
22 E. Rudberg, P. Sałek, T. Helgaker and H. Ågren, *J. Chem. Phys.*, 2005, **123**, 184108.
23 T. H. Dunning, *J. Chem. Phys.*, 1989, **90**, 1007–1023.
24 P. C. Hariharan and J. A. Pople, *Theor. Chim. Acta*, 1973, **28**, 213–222.
25 M. M. Francl, W. J. Pietro, W. J. Hehre, J. S. Binkley, M. S. Gordon, D. J. DeFrees and J. A. Pople, *J. Chem. Phys.*, 1982, **77**, 3654–3665.
26 P. A. M. Dirac, *Proc. R. Soc. London, Ser. A*, 1929, **123**, 714–733.
27 J. C. Slater, *Phys. Rev.*, 1951, **81**, 385–390.
28 S. H. Vosko, L. Wilk and M. Nusair, *Can. J. Phys.*, 1980, **58**, 1200–1211.
29 A. D. Becke, *Phys. Rev. A*, 1988, **38**, 3098–3100.
30 C. Lee, W. Yang and R. G. Parr, *Phys. Rev. B: Condens. Matter*, 1988, **37**, 785–789.
31 A. D. Becke, *J. Chem. Phys.*, 1993, **98**, 5648–5652.
32 J. P. Perdew, *Phys. Rev. B: Condens. Matter*, 1986, **33**, 8822–8824.
33 T. Clark, J. Chandrasekhar, G. W. Spitznagel and P. v. R. Schleyer, *J. Comput. Chem.*, 1983, **4**, 294–301.
34 *TURBOMOLE developer's version, a development of University of Karlsruhe and Forschungszentrum Karlsruhe GmbH, 1989-2007, TURBOMOLE GmbH, since 2007; available from* http://www.turbomole.com.
35 *DALTON, a molecular electronic structure program, Release 2.0 (2005), see* http://www.daltonprogram.org.
36 N. O. C. Winter and C. Hättig, *J. Chem. Phys.*, 2011, **134**, 184101.
37 D. E. Woon and T. H. Dunning, *J. Chem. Phys.*, 1993, **98**, 1358–1371.
38 F. Weigend, A. Köhn and C. Hättig, *J. Chem. Phys.*, 2002, **116**, 3175–3183.
39 A. Dreuw and M. Head-Gordon, *J. Am. Chem. Soc.*, 2004, **126**, 4007–4016.
40 P. Sałek, O. Vahtras, J. D. Guo, Y. Luo, T. Helgaker and H. Ågren, *Chem. Phys. Lett.*, 2003, **374**, 446–452.
41 S. Chakrabarti and K. Ruud, *Phys. Chem. Chem. Phys.*, 2009, **11**, 2592–2596.
42 L. De Boni, L. Misoguti, S. C. Zílio and C. R. Mendonça, *ChemPhysChem*, 2005, **6**, 1121–1125.
43 G. S. He, T.-C. Lin, J. Dai, P. N. Prasad, R. Kannan, A. G. Dombroskie, R. A. Vaia and L.-S. Tan, *J. Chem. Phys.*, 2004, **120**, 5275–5284.
44 S. Chakrabarti and K. Ruud, *J. Phys. Chem. A*, 2009, **113**, 5485.

 This journal is © the Owner Societies 2012